SCIENTIFIC REP⚙RTS

OPEN

Detection and control of charge states in a quintuple quantum dot

Takumi Ito[1,2,*], Tomohiro Otsuka[1,2,*], Shinichi Amaha[1], Matthieu R. Delbecq[1,2], Takashi Nakajima[1,2], Jun Yoneda[1,2], Kenta Takeda[1,2], Giles Allison[1], Akito Noiri[1,2], Kento Kawasaki[1,2] & Seigo Tarucha[1,2,3,4]

A semiconductor quintuple quantum dot with two charge sensors and an additional contact to the center dot from an electron reservoir is fabricated to demonstrate the concept of scalable architecture. This design enables formation of the five dots as confirmed by measurements of the charge states of the three nearest dots to the respective charge sensor. The gate performance of the measured stability diagram is well reproduced by a capacitance model. These results provide an important step towards realizing controllable large scale multiple quantum dot systems.

Quantum dots (QDs) are artificial systems in which electrons are confined in all three dimensions and the electronic states are determined by the confining potential and Coulombic interaction[1]. For multiple QDs the electronic states are furthermore influenced by the tunneling and interaction between dots. QDs can offer intriguing systems for constructing fermion Hubbard models[2] and also implementing elements of quantum computing[3–7]. Increasing the number of QDs is a necessary step towards these goals and has been attempted using various kinds of materials such as semiconductor heterostructures, nanowires[8,9] and self-assembled dots[10–12]. Single to quadruple QDs have been fabricated in semiconductor heterostrcuture[13–15] and applied to quantum bits using the charge or spin degree of freedom[16–22].
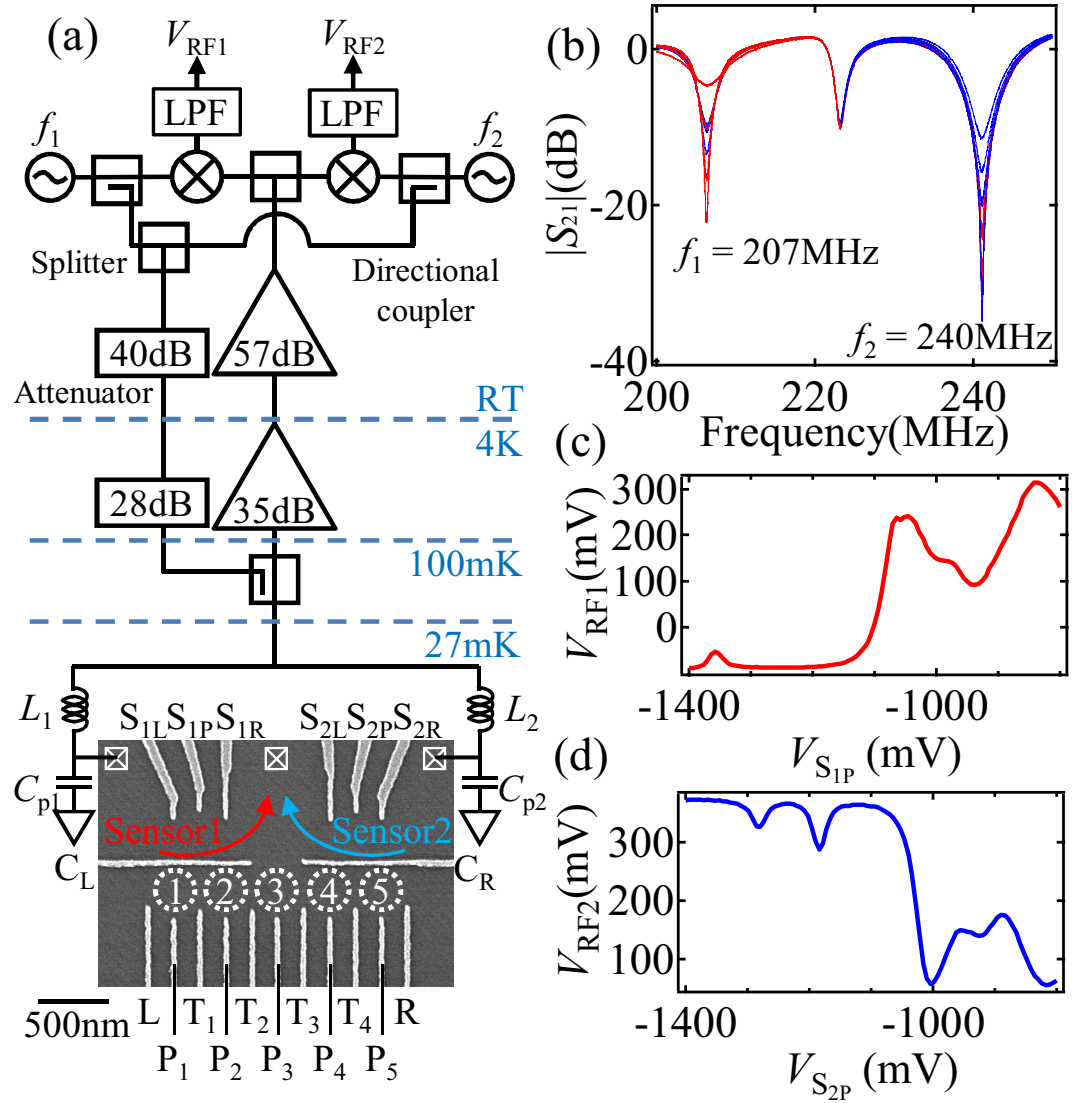
Scale-up of QD systems whose electronic states can be precisely manipulated and detected requires several technical advances. In the conventional device architecture, the electronic states are electrically manipulated by two plunger gates and detected by a single charge sensor[23–28]. Double or triple QDs (DQD or TQD) are the typical cases in which the charge states can be manipulated by two plunger gates attached to the two dots and detected by a charge sensor. This technique has been applied to quadruple QDs but not more, probably because the sensor sensitivity decreases with the distance to the target QD and also because more plunger gates must be appropriately adjusted to address the individual QDs. In addition multiple QDs are usually constructed by connecting dots in a row with a tunnel-coupled reservoir at each end. This geometry makes it difficult to load electrons from the reservoirs to the inner dots[29]. In general a set of two plunger gates, one charge sensor and two reservoirs is appropriate to address a triple QD. Therefore splitting into TQDs may be a straightforward approach to scale up the QD architecture[30,31].

In this work, we fabricate a semiconductor quintuple quantum dot (5QD) or series coupled five QDs with a concept relevant for further increasing the number of QDs. Our 5QD has a reservoir connected to the leftmost, center and rightmost dots, to facilitate loading of electrons to all dots. In addition, two RF charge sensors are independently and simultaneously operated using a frequency multiplexing technique[30] to complementarily and precisely read out the charge states. We modify the charge configuration with gate voltages to demonstrate the utility of this architecture by comparing the measured stability diagrams with capacitance model calculations[32].

Results

Device and measurement setup. Figure 1(a) shows a scanning electron micrograph of the device and a schematic of the measurement setup. By applying negative voltages to the gate electrodes, five QDs (QD_1 to QD_5), and two QD charge sensors (sensors 1 and 2) are formed at the dotted circles, and arrows, respectively. Sensors 1 and 2 can efficiently detect the three leftmost dots (QD_1 to QD_3), and the three rightmost (QD_3 to QD_5) dots, respectively. The plunger gate P_i tunes predominantly the energy level of QD_i, while the tunnel gate T_i tunes the tunnel coupling between QD_i and QD_{i+1}. To induce an additional reservoir coupling at QD_3, a gap is made in

Figure 1. (**a**) Scanning electron micrograph of the 5QD device and schematic of the measurement setup. (**b**) $|S_{21}|$ of the resonance circuit as a function of the carrier microwave frequency. The left (right) dip is caused by the resonator including sensor 1 (sensor 2). The center dip is caused by an unused resonator not connected to the device. The traces show the results with different conductance of the sensors (sensor 1 from 0.88 to 0.19 e^2/h and sensor 2 from 0.77 to 0.03 e^2/h). (**c**) ((**d**)) Changes of the RF signal from sensor1, V_{RF1}, as a function of $V_{S_{1P}}$ (**c**) and from sensor 2, V_{RF2} as a function of $V_{S_{2P}}$ (**d**).

the horizontal line gate (between C_L and C_R). Electrons are then loaded from the three reservoirs to all dots. This helps to initialize the charge states of the 5QD.

The QD charge sensors are connected to RF resonators configured by the inductors $L_1 = 270$ nH and $L_2 = 470$ nH and the stray capacitances C_{p1} and $C_{p2}(\approx 0.4$ pF) for the RF reflectometry. Figure 1(b) shows the reflected RF signal $|S_{21}|$ from the resonance circuit measured by the setup of Fig. 1(a). We observe dips caused by the resonance circuits including sensor 1 and sensor 2 at 207 MHz and 240 MHz respectively. We can detect the change of the sensor conductance through the reflected signal: $|S_{21}|$ at f_1 changes by 17 dB due to the conductance change of sensor 1 from 0.88 to 0.19 e^2/h (the red traces). Similarly the reflected signal at f_2 changes by 23 dB depending on the conductance change of sensor 2 from 0.77 to 0.03 e^2/h (the blue traces).

To read out the reflected signals at different frequencies, the room temperature part of the measurement circuit is configured by two sets of local oscillators and mixers (Fig. 1(a)). In this room temperature circuit, two RF carriers are combined and the reflected signal of each charge sensor is picked up by the mixer operating at each carrier frequency simultaneously. Note that simultaneous readout may be important for measurement of temporal correlation of charge or spin between different dots[33,34]. The changes of the RF signal from sensor 1 (V_{RF1}) and sensor 2 (V_{RF2}) are shown in Fig. 1(c) and (d) as a function of the sensor gate voltages $V_{S_{1P}}$ and $V_{S_{2P}}$ respectively. Note that due to a difference in phase, the reflected signals change in opposite directions in Fig. 1(d). In the
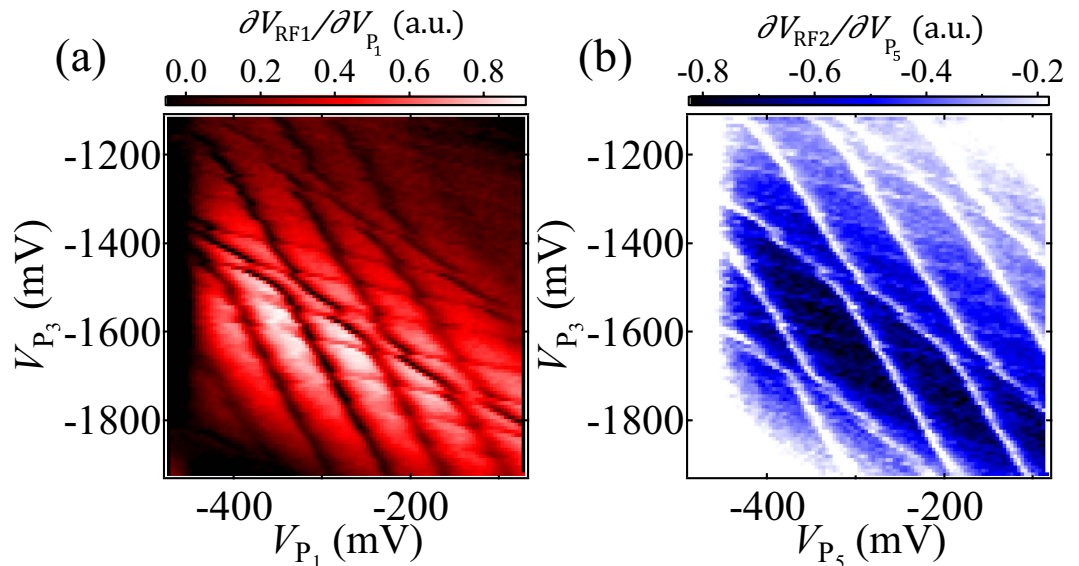
Figure 2. Stability diagram measured for QD_1 to QD_3 in $\partial V_{RF1}/\partial V_{P_1}$ as a function of V_{P_1} and V_{P_3} (**a**) and for QD_3 to QD_5 in $\partial V_{RF2}/\partial V_{P_5}$ as a function of V_{P_5} and V_{P_3} (**b**). At the center of each stability diagram all plunger gate voltage conditions are $V_{P_1} = -286$ mV, $V_{P_2} = -1140$ mV, $V_{P_3} = -1120$ mV, $V_{P_4} = -1260$ mV and $V_{P_5} = -298$ mV. The 5QD can be tuned by separating it into two TQDs since QD_3 is contacted to the lead.

following measurement, gate voltages $V_{S_{1P}}$ and $V_{S_{2P}}$ are adjusted to the condition most sensitive to electrostatic changes of the surrounding environment.

Tuning of the 5QD. Gate tuning of the 5QD is simplified by splitting the five QDs into two TQDs and manipulating the charge states on the two different stability diagrams. Figure 2 shows the numerical derivative of the RF reflectometry signal measured by sensor 1, $\partial V_{RF1}/\partial V_{P_1}$, in the $V_{P_1}-V_{P_3}$ plane (a) and by sensor 2, $\partial V_{RF2}/\partial V_{P_5}$, in the $V_{P_5}-V_{P_3}$ plane (b), respectively. In each diagram, we observe three sets of distinct charge transition lines with three different slopes, which are defined by the capacitive couplings between the dots and the modulating gates. Each set of charging lines (from the more horizontal to the more vertical) is assigned to charging QD_1 to QD_3 in (a) and QD_5 to QD_3 in (b). We adjust the voltages on V_{T_1}, V_{T_2}, V_{T_3} and V_{T_4} to make all tunnel or electrostatic couplings between adjacent dots roughly the same judging from the size of avoided crossings between two different charge transition lines. Here we confirm that couplings between distant dots are small, because the corresponding charging lines just cross with each other with no anticrossing. Since the two diagrams share a common P_3 axis in the same range, we are able to evaluate appropriate voltages of all gates to manipulate the charge state of the 5QD.

Stability diagram of the 5QD. We use the gate voltage setting derived from Fig. 2 as a guide to establish the stability diagram of the 5QD. Figure 3(a) and (b) show the diagram in the plane of V_{P_1} and V_{P_5} measured using sensor 1 ($\partial V_{RF1}/\partial V_{P_1}$) and 2 ($\partial V_{RF2}/\partial V_{P_1}$), respectively. The other gate voltages are fixed at $V_{P_2} = -1585$ mV, $V_{P_3} = -1020$ mV, and $V_{P_4} = -470$ mV. The values of V_{T_1} to V_{T_4} are the same as used in Fig. 2. In both figures, five sets of charge transition lines with different slopes are distinguished and from the slopes we are able to assign them to charging five different dots: QD_1 to QD_5 from vertical to horizontal. The difference in the spacing of the charge transition lines of QD_1 and QD_5 is caused by the difference in the lever arm of the gates or the charging energy. Figure 3(a) and (b) are measured simultaneously using the multiplex technique of RF reflectometry. Note the charge transition lines of QD_1 to QD_3 are clearly visible whereas those of QD_4 and QD_5 are less visible in Fig. 3(a). In contrast the charging lines of QD_3 to QD_5 are more visible in Fig. 3(b). This observation indicates that each sensor is sensitive to charging of at least three nearest QDs and that two sensors can together detect all charge transitions of the 5QD. Note that the dots in Fig. 3(a) and (b) are not in a few electron regime due to limitation of the gate voltage range and contain dozens of electrons judging from the spacing of the charge transition lines[14]. Also QD_3 has the most electrons due to the gate electrode design. We will be able to reduce the number of electrons by reducing the gaps between the gates to form smaller dots.

In Fig. 3(c) we show the charging lines for the 5QD by plotting the data points of the dark and white lines in Fig. 3(a) and (b): red and blue points from (a) and (b) and green points from both. Avoided crossings of charging lines of neighboring QDs indicate finite capacitive coupling among all five QDs as is the case in Fig. 2. Also, none of the charge transition lines are fragmented, suggesting that tunneling rates are kept sufficiently high for all QDs. Note that charge sensors are tuned to be most sensitive at the center of stability diagrams and become insensitive in the upper right region (grey region of Fig. 3(c)).

In large systems of multiple QDs, the charge states become complicated and difficult to discriminate. Therefore numerical calculations of stability diagrams are helpful in the process of adjusting gate voltages to search for
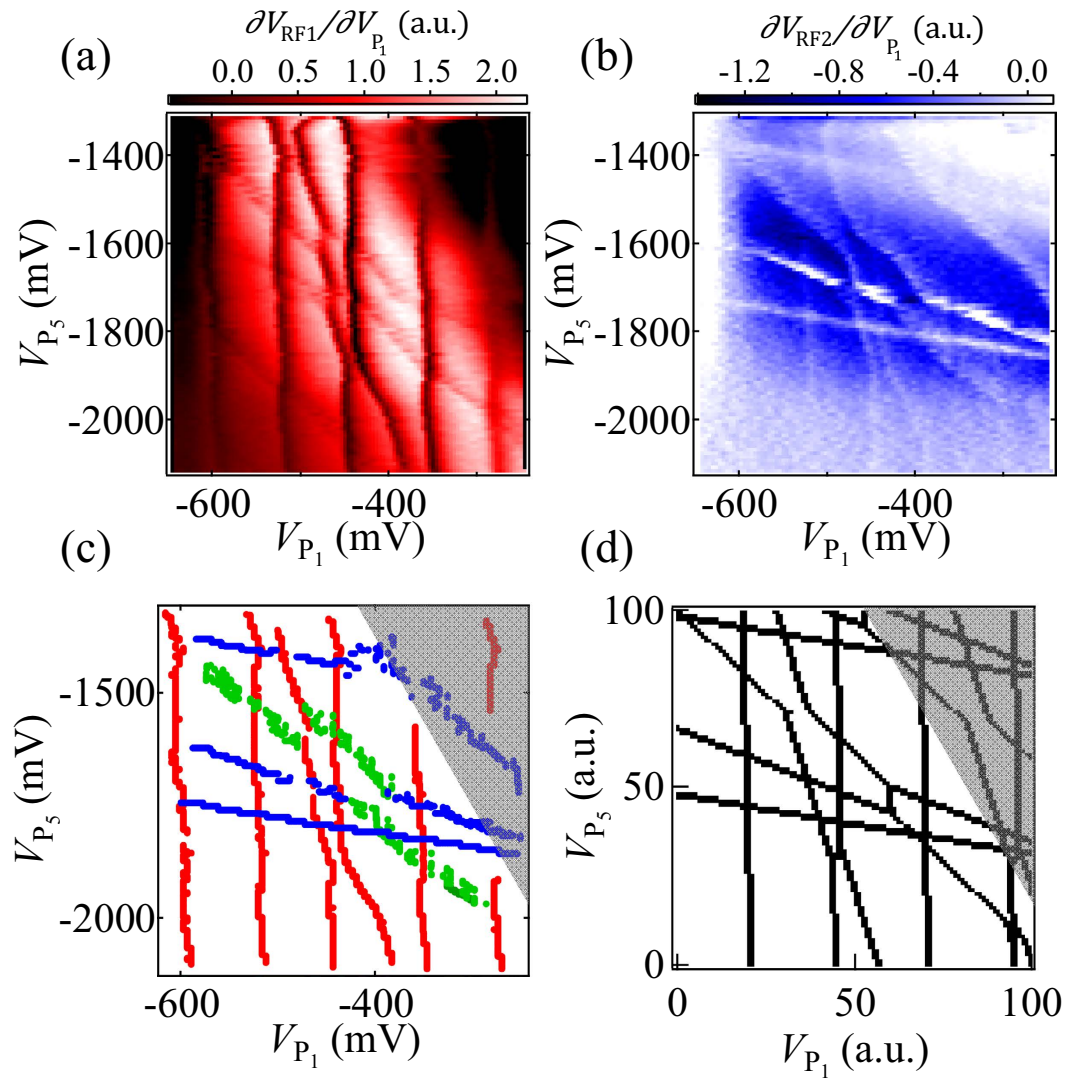
Figure 3. Stability diagram in the plane of V_{P_1} and V_{P_5} for the 5QD measured simultaneously using the multiplex technique: $\partial V_{RF1}/\partial V_{P_1}$ (**a**) and $\partial V_{RF2}/\partial V_{P_1}$ (**b**) with $V_{P_2} = -1585\,\text{mV}$, $V_{P_3} = -1020\,\text{mV}$, and $V_{P_4} = -470\,\text{mV}$. (**c**) Data points extracted from the charge transition lines in (**a**) and (**b**): Red, or blue points from (**a**), or (**b**), respectively. The grey region shows the area where the sensor sensitivity is too low to apparently distinguish the transition lines. (**d**) Calculated stability diagram using the capacitive QD model. The capacitance values are estimated from the experiments.

desirable charge states. We find that the charge stability diagram obtained here is well reproduced in a qualitative manner using a capacitive QD model[15,35]. Figure 3(d) is the calculated stability diagram to reproduce the experiment of Fig. 3(c). The ratios of the capacitance used in the calculation are all taken from the experiment. This simple model shows good agreement with the experiment in which the dots contain many electrons and when we focus on a limited range of the charge stability diagram. We see that the main features in Fig. 3(c) are well reproduced by the calculation (Fig. 3(d)).

Tunability of the 5QD device. Finally we demonstrate the tunability of this device. Figure 4(a) and (c) are the $V_{P_1} - V_{P_5}$ stability diagrams measured for two different V_{P_3} values of $-1000\,\text{mV}$, and $-1040\,\text{mV}$, respectively but keeping other gate voltage values the same as in Fig. 3(c). The charge transition line of QD$_3$ highlighted in red shifts more than the other charge transition lines. This shift is well reproduced by the calculation of Fig. 4(b) and (d). In the same way, Fig. 4(e) and (g) are the diagrams measured for two different values of V_{P_4} of $-450\,\text{mV}$ and $-490\,\text{mV}$, respectively. The charging line of QD$_4$ highlighted in red shifts more than the others as expected from the calculation of Fig. 4(f) and (h).

Conclusion
In conclusion, we have fabricated a 5QD device with an additional contact to the center dot from a reservoir and two RF charge sensors, whose design suits further increasing of the number of QDs. We have characterized the
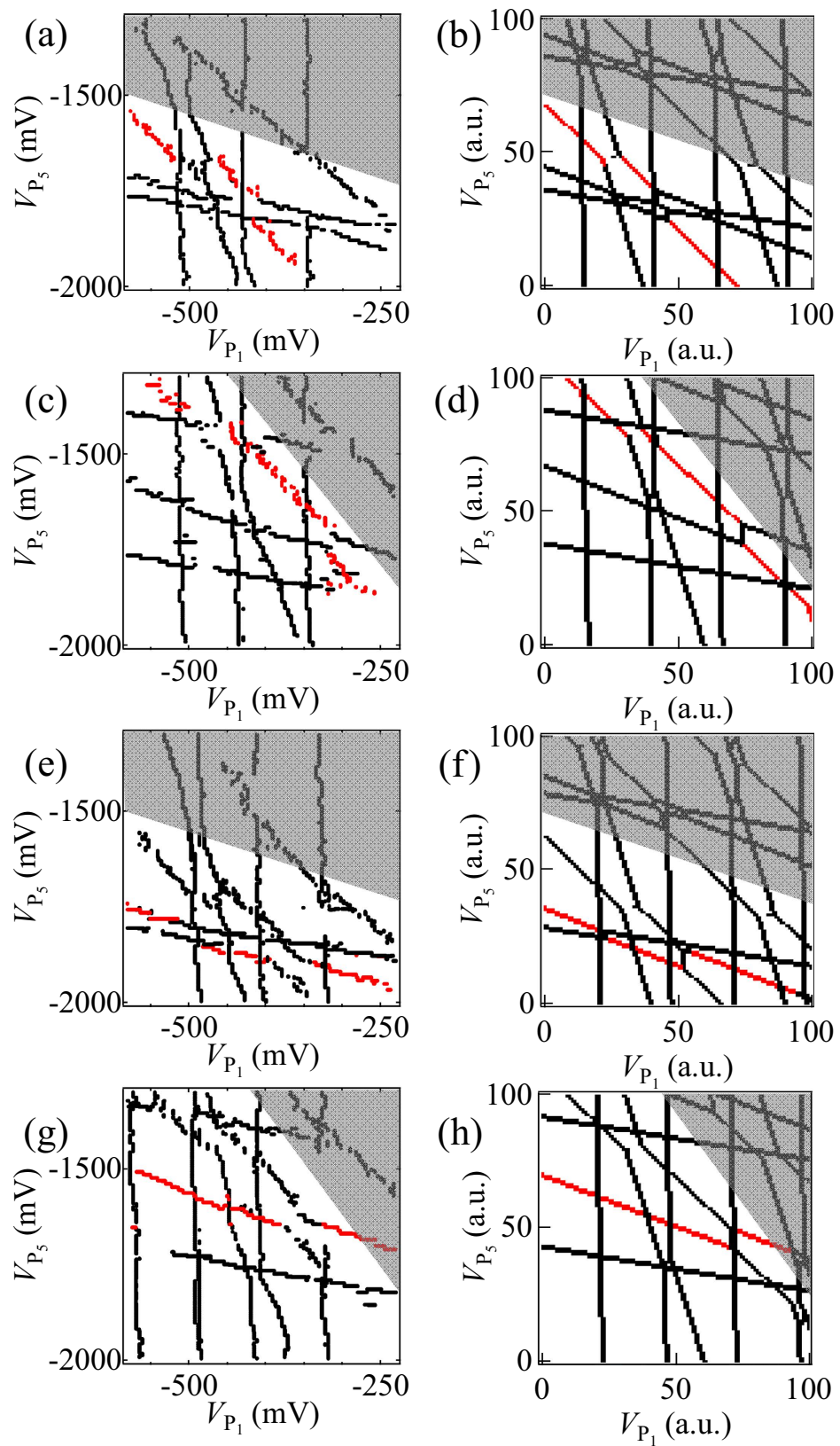
Figure 4. Comparison between the measured ((**a**), (**c**), (**e**) and (**g**)) and calculated ((**b**), (**d**), (**f**) and (**h**)) stability diagrams in the plane of V_{P_1} and V_{P_5} with V_{P_3} and V_{P_4} as parameters: $V_{P_3} = -1000\,\text{mV}$ and $V_{P_4} = -470\,\text{mV}$ in (**a**) and (**b**); $V_{P_3} = -1040\,\text{mV}$ and $V_{P_4} = -470\,\text{mV}$ in (**c**) and (**d**); $V_{P_3} = -1020\,\text{mV}$ and $V_{P_4} = -450\,\text{mV}$ in (**e**) and (**f**); $V_{P_3} = -1020\,\text{mV}$ and $V_{P_4} = -490\,\text{mV}$ in (**g**) and (**h**). The grey region shows the area where some charging lines are not distinguished due to the low sensor sensitivity.

gate performance on the charge state stability diagram and well distinguished the charge transition lines corresponding to all five dots thanks to the use of the two charge sensors. We have demonstrated that the gate performance on the stability diagram is well reproduced by the capacitance model. These results are important steps for further scale up of QD system.

Methods

Device structure and measurement. The device was fabricated from a GaAs/AlGaAs heterostructure wafer with an electron sheet carrier density of 5.6×10^{15} m^{-2} and a mobility of 17 m^2/Vs. The two-dimensional electron gas is formed 60 nm under the wafer surface. We patterned a mesa by wet-etching and formed Ti/Au Schottky surface gates by metal deposition, which appear white in Fig. 1(a). All measurements were conducted in a dilution fridge cryostat at a temperature of 27 mK.

References

1. Kouwenhoven, L. P., Marcus C. M., McEuen P. L., Tarucha S., Westervelt R. M. & Wingreen, N. S. Electron Transport in Quantum Dots. *Proc. Adv. Study Inst. Mesoscopic Electron* **345**, 105–204 (1997).
2. Byrnes, T., Kim, N. Y., Kusudo, K. & Yamamoto, Y. Quantum simulation of Fermi-Hubbard models in semiconductor quantum-dot arrays. *Phys. Rev. B* **78**, 075320 (2008).
3. DiVincenzo, D. P. Quantum Compuration. *Science* **270**, 255–261 (1995).
4. Loss, D. & DiVincenzo, D. P. Quantum computation with quantum dots. *Physical Review A* **57**, 120–126 (1998).
5. Taylor, J. M. *et al.* Fault-tolerant architecture for quantum computation using electrically controlled semiconductor spins. *Nat. Phys.* **1**, 177–183 (2005).
6. Hanson, R., Kouwenhoven, L. P., Petta, J. R., Tarucha, S. & Vandersypen, L. M. K. Spins in few-electron quantum dots. *Rev. Mod. Phys.* **79**, 1217–1265 (2007).
7. Kloeffel, C. & Loss, D. Prospects for Spin-Based Quantum Computing in Quantum Dots. *Annu. Rev. Condens. Matter Phys.* **4**, 51–81 (2013).
8. Björk, M. T. *et al.* Few-electron quantum dots in nanowires. *Nano Lett.* **4**, 1621–1625 (2004).
9. Fasth, C., Fuhrer, A., Björk, M. T. & Samuelson, L. Tunable double quantum dots in inAs nanowires defined by local gate electrodes. *Nano Lett.* **5**, 1487–1490 (2005).
10. Cusack, M. A., Briddon, P. R. & Jaros, M. Electronic structure of InAs/GaAs self-assembled quantum dots. *Phys. Rev. B* **54**, R2300 (1996).
11. García, J. M., Mankad, T., Holtz, P. O., Wellman, P. J. & Petroff, P. M. Electronic states tuning of InAs self-assembled quantum dots. *Appl. Phys. Lett.* **72**, 3172–3174 (1998).
12. Fonseca, L. R. C., Jimenez, J. L. & Leburton, J. P. Electronic coupling in InAs/GaAs self-assembled stacked double-quantum-dot systems. *Phys. Rev. B* **58**, 9955–9960 (1998).
13. Thalineau, R., Valentin, S. R., Wieck, A. D., Bäeuerle, C. & Meunier, T. Interplay between exchange interaction and magnetic field gradient in a double quantum dot with two individual electron spin qubits. *Phys. Rev. B* **90**, 075436 (2014).
14. Takakura, T. *et al.* Single to quadruple quantum dots with tunable tunnel couplings. *Appl. Phys. Lett.* **104**, 113109 (2014).
15. Delbecq, M. R. *et al.* Full control of quadruple quantum dot circuit charge states in the single electron regime. *Appl. Phys. Lett.* **104**, 183111 (2014).
16. Petta, J. R. *et al.* Coherent Manipulation of Coupled Electron Spins in Semiconductor Quantum Dots. *Science* **309**, 2180–2184 (2005).
17. Koppens, F. H. L. *et al.* Driven coherent oscillations of a single electron spin in a quantum dot. *Nature* **442**, 766–771 (2006).
18. Takakura, T. *et al.* Triple quantum dot device designed for three spin qubits. *Appl. Phys. Lett.* **97**, 212104 (2010).
19. Medford, J. *et al.* Quantum-Dot-Based Resonant Exchange Qubit. *Phys. Rev. Lett.* **111**, 050501 (2013).
20. Shulman, M. D. *et al.* Demonstration of Entanglement of Electrostatically Coupled Singlet-Triplet Qubits. *Science* **336**, 202–205 (2012).
21. Yoneda, J. *et al.* Fast Electrical Control of Single Electron Spins in Quantum Dots with Vanishing Influence from Nuclear Spins. *Phys. Rev. Lett.* **113**, 267601 (2014).
22. Otsuka, T. *et al.* Single-electron Spin Resonance in a Quadruple Quantum Dot. *Sci. Rep.* **6**, 31820 (2016).
23. Field, M. *et al.* Measurements of Coulomb blockade with a noninvasive voltage probe. *Phys. Rev. Lett.* **70**, 1311–1314 (1993).
24. Schoelkopf, R. J., Wahlgren, P., Kozhevnikov, A. A., Delsing, P. & Prober, D. E. The Radio-Frequency Single-Electron Transistor (RF-SET): A Fast and Ultrasensitive Electrometer. *Science* **280**, 1238–1242 (1998).
25. Reilly, D. J., Marcus, C. M., Hanson, M. P. & Gossard, A. C. Fast single-charge sensing with a rf quantum point contact. *Appl. Phys. Lett.* **91**, 162101 (2007).
26. Cassidy, M. C. *et al.* Single shot charge detection using a radio-frequency quantum point contact. *Appl. Phys. Lett.* **91**, 222104 (2007).
27. Müller, T. *et al.* A Radio Frequency Quantum Point Contact Charge Read-Out. *AIP Conf. Proc.* **893**, 1113–1114 (2007).
28. Barthel, C. *et al.* Fast sensing of double-dot charge arrangement and spin state with a radio-frequency sensor quantum dot. *Phys. Rev. B* **81**, 161308 (2010).
29. Gaudreau, L. *et al.* A tunable few electron triple quantum dot. *Appl. Phys. Lett.* **95**, 193101 (2009).
30. Laird, E. A. *et al.* Coherent spin manipulation in an exchange-only qubit. *Phys. Rev. B* **82**, 075403 (2010).
31. Hornibrook, J. M. *et al.* Frequency multiplexing for readout of spin qubits. *Appl. Phys. Lett.* **104**, 103108 (2014).
32. Baart, T. A., Eendebak, P. T., Reichl, C., Wegscheider, W. & Vandersypen, L. M. K. Computer-automated tuning of semiconductor double quantum dots into the single-electron regime. *Appl. Phys. Lett.* **108**, 213104 (2016).
33. Braakman, F. R., Barthelemy, P., Reichl, C., Wegscheider, W. & Vandersypen, L. M. K. Long-distance coherent coupling in a quantum dot array. *Nat. Nanotechnol.* **8**, 432–437 (2013).
34. Srinivasa, V., Xu, H. & Taylor, J. M. Tunable Spin-Qubit Coupling Mediated by a Multielectron Quantum Dot. *Phys. Rev. Lett.* **114**, 226803 (2015).
35. van der Wiel, W. G. *et al.* Electron transport through double quantum dots. *Rev. Mod. Phys.* **75**, 1–22 (2003).

Acknowledgements

Author Contributions

T. I., T. O., S. A., M. D., T. N., J. Y., K. T., G. A. and S. T. planned the project; T. O., S. A., M. D. and T. N. performed device fabrication; all authors conducted experiments and data analysis; all authors discussed the results; T. I., T. O., S. A., M. D., T. N., J. Y., K. T., G. A. and S. T. wrote the manuscript.

Additional Information

Competing financial interests: The authors declare no competing financial interests.

How to cite this article: Ito, T. *et al.* Detection and control of charge states in a quintuple quantum dot. *Sci. Rep.* **6**, 39113; doi: 10.1038/srep39113 (2016).

Publisher's note: Springer Nature remains neutral with regard to jurisdictional claims in published maps and institutional affiliations.